Table 2. Biodistribution of radioactivity after intravenous injection of ^{111}In-DTPA-Ac-TZ14011 in nude mice bearing pancreatic carcinoma, AsPC-1

	1 h	6 h	24 h	1h + Ac-TZ14011 [d]
Blood [a]	0.39 (0.06)	0.05 (0.01)	0.03 (0.01)	2.06** (0.61)
Liver [a]	27.0 (2.9)	25.2 (2.0)	19.3 (2.5)	1.95** (0.25)
Kidney [a]	50.9 (4.3)	43.4 (6.3)	29.5 (5.7)	45.4 (6.8)
Spleen [a]	8.22 (0.70)	7.57 (0.54)	5.83 (0.99)	2.66** (1.21)
Pancreas [a]	0.15 (0.03)	0.05 (0.01)	0.05 (0.02)	1.07** (0.46)
Muscle [a]	0.17 (0.05)	0.07 (0.02)	0.07 (0.01)	1.35** (0.26)
Tumor [a]	0.51 (0.08)	0.20 (0.03)	0.14 (0.03)	1.70** (0.27)
T/B ratio [b]	1.31 (0.14)	4.05 (0.79)	5.65 (2.89)	0.88* (0.31)
T/M ratio [c]	3.17 (0.99)	4.43 (1.89)	3.23 (1.08)	1.31** (0.41)

Each value represents the mean (SD) for five animals.

[a] Expressed as % injected dose per gram, [b] Tumor-to-blood ratio, [c] Tumor-to-muscle ratio, [d] Co-injection with unlabeled Ac-TZ14011 (10 mg/kg).

* p <0.05, ** p < 0.005, comparison between ^{111}In-DTPA-Ac-TZ14011 with or without unlabeled Ac-TZ14011 at 1 h.

FIGURE LEGENDS

Fig. 1. Structures of T140 and Ac-TZ14011. There are four amino acid residues indispensable for the antagonistic activity (blue residues) which formed the pharmacophore. Nal: L-3-(2-naphthyl)alanine, Cit: L-citrulline. Ac-TZ14011 has a single amino group (D-Lys^{8}) for site-selective conjugation of radiolabels, which is distant from the pharmacophore.

Fig. 2. Synthesis of In-DTPA-Ac-TZ14011. Reagents: (a) stepwise elongation; (b) acetic anhydride, pyridine; (c) trifluoroacetic acid, thioanisole, *m*-cresol, 1,2-ethanedithiol; (d) air-oxidation; (e) *N*-hydroxysuccinimide, *N,N*-dicyclohexylcarbodiimide; (f) trifluoroacetic acid; (g) $InCl_3 \cdot 4H_2O$.

Fig. 3. Reversed-phase HPLC profiles of nonradioactive In-DTPA-Ac-TZ14011 (solid line), DTPA-Ac-TZ14011 (broken line) (A) and ^{111}In-DTPA-Ac-TZ14011 (B).

Figure 1

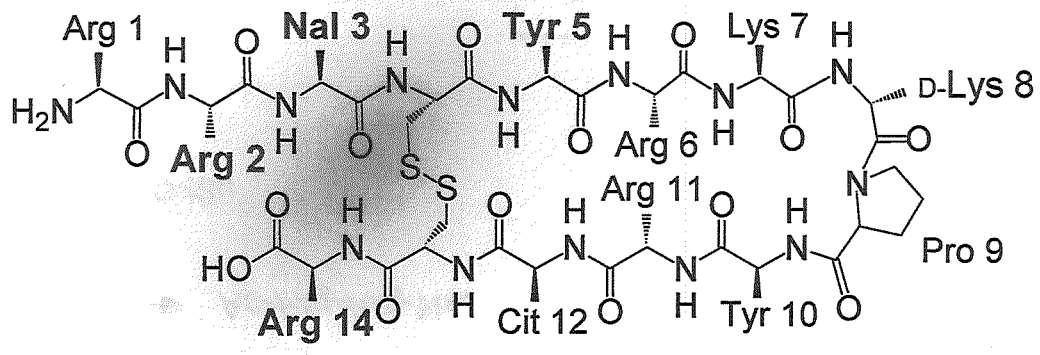

T140

Pharmacophore

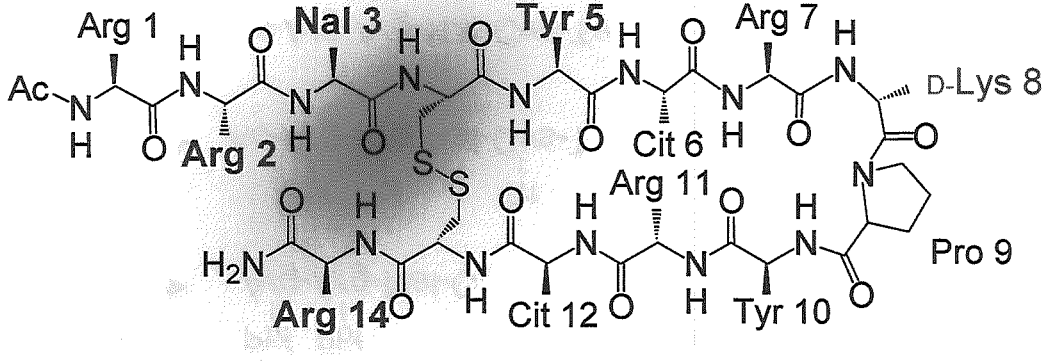

Ac-TZ14011

Figure 2

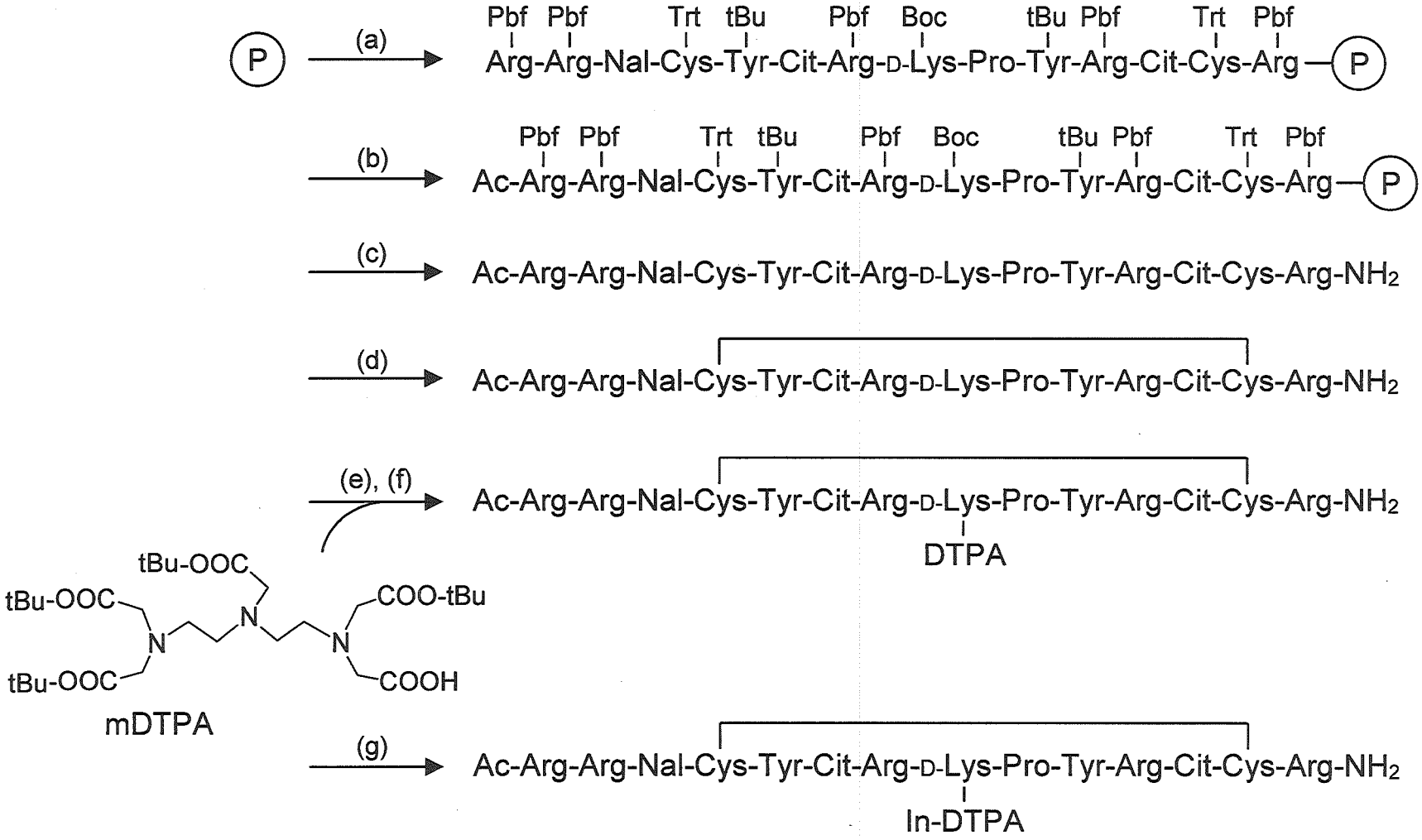

(P) : 4-(2',4'-dimethoxyphenylaminomethyl)phenoxy (SAL) resin

Figure 3

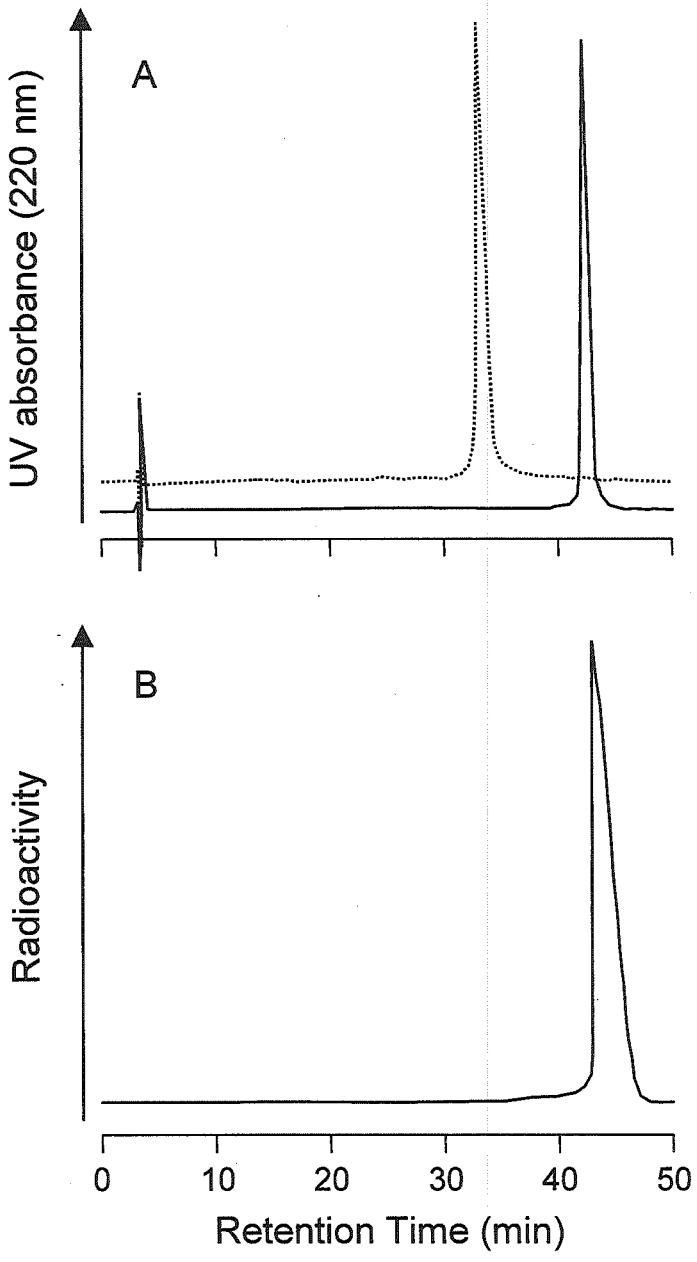
A
UV absorbance (220 nm)
B
Radioactivity
0
10
20
30
40
50
Retention Time (min)

Enhanced Apoptotic Reaction Correlates with Suppressed Tumor Glucose Utilization After Cytotoxic Chemotherapy: Use of ^{99m}Tc-Annexin V, ^{18}F-FDG, and Histologic Evaluation

Toshiki Takei, MD[1]; Yuji Kuge, PhD[2]; Songji Zhao, MD[2]; Masayuki Sato, BS[3]; H. William Strauss, MD[4]; Francis G. Blankenberg, MD[5]; Jonathan F. Tait, MD, PhD[6]; and Nagara Tamaki, MD[1]

[1]Department of Nuclear Medicine, Graduate School of Medicine, Hokkaido University, Sapporo, Japan; [2]Department of Tracer Kinetics, Graduate School of Medicine, Hokkaido University, Sapporo, Japan; [3]Department of Radiopharmaceutical Chemistry, Health Sciences University of Hokkaido, Tobetsu, Japan; [4]Department of Nuclear Medicine, Memorial Sloan–Kettering Cancer Center, New York, New York; [5]Division of Nuclear Medicine, Department of Radiology, Stanford University School of Medicine, Stanford, California; and [6]Department of Laboratory Medicine, University of Washington, Seattle, Washington

Cancer chemotherapy enhances the apoptosis, whereas apoptosis is a suicidal mechanism requiring energy. We determined the relationship between apoptosis and glucose utilization during cancer chemotherapy using ^{99m}Tc-annexin V (^{99m}Tc-annexin A5) and ^{18}F-FDG and compared their uptake with histologic findings in a rat tumor model. **Methods:** Allogenic hepatoma cells (KDH-8) were inoculated into the left calf muscle of male Wistar rats (WKA). Eleven days after the inoculation, the rats were randomly divided into 3 groups: The first group (n = 7) received a single dose of gemcitabine (90 mg/kg, intravenously), the second group (n = 8) received cyclophosphamide (150 mg/kg, intraperitoneally), and the third group (n = 7) was untreated and served as the control group. We injected ^{99m}Tc-annexin V 48 h after the chemotherapy and then injected ^{18}F-FDG to all rats 1 h before sacrifice. Six hours after ^{99m}Tc-annexin V injection, the rats were sacrificed and the organs, including the tumor, were removed and radioactivity was counted. The radioactivities of ^{18}F and ^{99m}Tc in the organs were determined using normalization by tissue weight. Histologic evaluation by the terminal deoxynucleotidyl transferase-mediated deoxyuridine triphosphate nick-end labeling (TUNEL) method and the immunostaining of glucose transporter-1 (GLUT-1) were also performed to obtain the indices of apoptosis and glucose utilization, respectively. The rate of positively stained cells was calculated and analyzed statistically. **Results:** After chemotherapy using gemcitabine and cyclophosphamide, the ^{99m}Tc-annexin V uptake (percentage injected dose per gram × kg [(%ID/g) × kg]; mean ± SD) in tumor increased significantly (0.062 ± 0.012 (%ID/g) × kg in the gemcitabine-treated group and 0.050 ± 0.012 (%ID/g) × kg in the cyclophosphamide group vs. 0.031 ± 0.005 (%ID/g) × kg in the control group; $P < 0.01$). In contrast, the ^{18}F-FDG in tumor decreased significantly (0.483 ± 0.118 (%ID/g) × kg in the gemcitabine group and 0.583 ± 0.142 (%ID/g) × kg in the cyclophosphamide group) compared with that in the control group (0.743 ± 0.084 (%ID/g) × kg; $P < 0.01$). In addition, ^{18}F-FDG uptake in tumor negatively correlated with ^{99m}Tc-annexin V uptake ($r = -0.75$; $P < 0.01$). In the gemcitabine and cyclophosphamide groups, the rate of TUNEL positively stained cells was significantly higher than that in the control group (10.2% ± 1.7% and 8.0% ± 1.5% vs. 5.2% ± 1.5%; $P < 0.01$), whereas the GLUT-1 expression level showed no definite changes in histologic analyses. **Conclusion:** These data indicate that an enhanced apoptotic reaction correlated with suppressed tumor glucose utilization after cytotoxic chemotherapy as determined using radiotracers and histologic evaluation. The increase in ^{99m}Tc-annexin V and the decrease in ^{18}F-FDG in tumor can be useful markers for predicting therapeutic outcomes and for prognosis at the early stage of chemotherapy.

Key Words: molecular imaging; ^{18}F-FDG; ^{99m}Tc-annexin V; apoptosis; cancer chemotherapy

J Nucl Med 2005; 46:794–799

Apoptosis, or programmed cell death, is activated in the course of successful antineoplastic therapy (*1–3*). Determining baseline levels of apoptosis and the increment of apoptosis induced by therapy can serve as useful prognostic markers (*4,5*). Cancer chemotherapy with agents such as 2′,2′-difluoro-2′-deoxycytidine (gemcitabine) and cyclophosphamide not only arrest metabolism and induce DNA alkylation, respectively, but also enhance apoptosis (*6,7*). Early in the course of apoptosis, phosphatidylserine (PS) is expressed on the external leaflet of the cell membrane. Annexin V (annexin A5), a human protein with a high affinity for membrane-bound PS, can be labeled with ^{99m}Tc for in vivo imaging of apoptosis (*8*). In an earlier study, we used this imaging technique to quantify the time course and

Received Sep. 11, 2004; revision accepted Dec. 8, 2004.

For correspondence or reprints contact: Nagara Tamaki, MD, Department of Nuclear Medicine, Graduate School of Medicine, Hokkaido, University, Kita 15 Nishi 7, Kita-ku, Sapporo 060-8638, Japan.

E-mail: natamaki@med.hokudai.ac.jp

intensity of apoptosis induced by treatment with cyclophosphamide (*7,9,10*).

Because apoptosis requires energy to destroy cellular DNA and produce apoptosomes, evaluating cellular metabolism in the course of apoptosis may identify the process with an increase in substrate consumption. Since glucose is a major substrate for tumor cells, serial images recorded with the glucose analog ^{18}F-FDG may be useful for this purpose. Although ^{18}F-FDG PET is widely applied for clinical staging, differential diagnosis, therapy monitoring, detecting recurrence, and prognostic prediction of malignant diseases (*11,12*), clinical studies typically demonstrate a decrease in ^{18}F-FDG uptake before morphologic regression after appropriate chemotherapeutic regimens. Furthermore, the degree of initial metabolic suppression by chemotherapy can be correlated with the therapeutic outcomes such as malignant lymphoma or head and neck cancer (*13,14*).

This study was undertaken to compare the apoptotic response with the metabolic response in animals with implanted hepatomas and to determine the relative sensitivity of each approach to identify successful treatment.

MATERIALS AND METHODS

Preparation of Animal Models

All procedures involving animals were performed in accordance with institutional guidelines (Guide for the Care and Use of Laboratory Animals of Hokkaido University). KDH-8 is a rat transplantable hepatocellular carcinoma induced by 3′-methyl-4-dimethylaminoazobenzene in Wistar King Aptekman/Hok (WKA/H) rats (supplied by the Experimental Animal Institute, Graduate School of Medicine, Hokkaido University, Sapporo) and maintained in vivo by intraperitoneal passage every 5 d (supplied by the Department of Pathologic Oncology, Graduate School of Medicine, Hokkaido University, Sapporo). KDH-8 rat allogenic hepatoma cells (1×10^6 cells per rat) were inoculated into the left calf muscle of 8-wk-old male WKA/H rats (*7,15*). No obvious rejection or graft-versus-host reaction was observed. Our previous study showed a high uptake of ^{18}F-FDG and high expression of GLUT-1 in this KDH-8 rat tumor (*16*). Cyclophosphamide (Endoxan; Baxter) and gemcitabine (GEMZAR; Eli Lilly) were each dissolved in saline for injection. Eleven days after the intramuscular injection of KDH-8 tumor cells, rats, which weighed 187–253 g (measuring about 15 mm in diameter), with palpable tumors were randomly divided into 3 groups. The first group (n = 7) was treated with a single dose of gemcitabine (90 mg/kg, intravenously), the second group (n = 8) was treated with a single dose of cyclophosphamide (150 mg/kg, intraperitoneally), and the third group (n = 7) was untreated (control group) (*7,17*). All rats were anesthetized with pentobarbital (0.025 mg/kg, intraperitoneally) when these treatments were undertaken.

Methods Using Radioactive Tracers and Determining Biodistribution

Human annexin V was produced by expression in *Escherichia coli* as described (*8,18–21*). Annexin V was derivatized with hydrazinonicotinamide (HYNIC) and then labeled with ^{99m}Tc with tricine as coligand as described (*8*) to a specific activity of 3.0 MBq/μg protein. Rats were fasted overnight before sacrifice. ^{99m}Tc-Annexin V (37 MBq) was injected intravenously approximately 48 h after chemotherapy. The animals were under pentobarbital anesthesia at the time of radiopharmaceutical injection. One hour before sacrifice, 20 MBq of ^{18}F-FDG were injected intravenously. The radiopharmaceuticals were injected intravenously into the coccygeal vein. The blood sugar level was measured immediately before ^{18}F-FDG injection (BS1) and immediately before sacrifice (BS2). Six hours after the ^{99m}Tc-annexin V injection (1 h after ^{18}F-FDG injection), the rats were sacrificed by whole-blood sampling under ether inhalation anesthesia. The tumor, an aliquot of blood, and the contralateral femoral muscle were removed, cleaned, and weighed; radioactivity was determined using an automatic γ-counter (1480 WIZARDTM3″; Wallac Co., Ltd.). First, ^{18}F activity was measured (energy peak, 511 keV ± 20%). After >24 h for decay of ^{18}F, ^{99m}Tc activity was determined (energy peak, 140 keV ± 20%). A time-line diagram of this study is shown in Figure 1.

Activity in each window was compared with an aliquot of the injected dose to permit calculation of percentage uptake/gram of tissue after normalization to the rat's weight ((%ID/g) × kg). The tumor samples were divided into 3 parts. Using aliquots of the tumor tissues, formalin-fixed, paraffin-embedded specimens then were prepared for subsequent histologic studies. The tumor-to-muscle ratio (T/M ratio) and the tumor-to-blood ratio (T/B ratio) were calculated from the (%ID/g) × kg value in each tissue (*7,10,15*).

Histologic Evaluation

Apoptotic cells were determined by hematoxylin and eosin staining and the direct immunoperoxidase detection of digoxigenin-labeled 3′ DNA strand breaks by the use of the terminal deoxynucleotidyl transferase-mediated deoxyuridine triphosphate nick-end labeling (TUNEL) method. The formalin-fixed, paraffin-embedded tissues were sectioned at 3-μm thickness. TUNEL was performed according to a standard procedure using a commercially available kit (Apoptosis in situ Detection Kit; Wako Pure Chemical Industries, Ltd.).

The expression of glucose transporter-1 (GLUT-1) in adjacent slices was examined according to a standard immunostaining

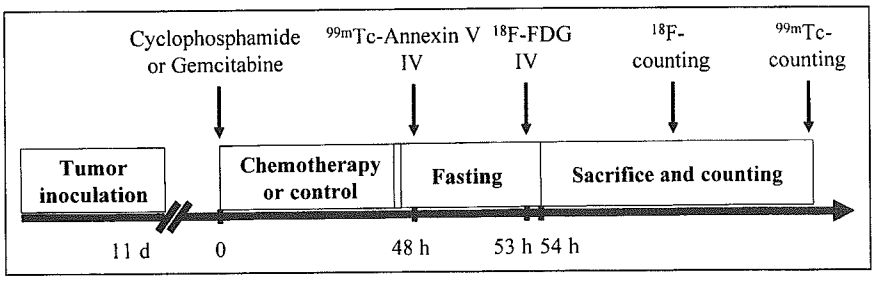

FIGURE 1. Time-line diagram of this study. IV = intravenously.

procedure. Deparaffinized sections were incubated with an anti–GLUT-1 antibody (Chemicon International, Inc.) at 37°C. The bound antibody was visualized using the avidin/biotin conjugate immunoperoxidase procedure with a HISTOFINE SAB-PO kit (Nichirei) and 3,3′-diaminobenzine tetrahydrochloride.

TUNEL and GLUT-1 positively stained cells were counted in 10 randomly selected high-power (×200) fields (with no knowledge of the treatment to avoid experimental bias) (*7,10,15*). The rate of TUNEL positively stained cells was determined by calculating the average percentage. The expression level of GLUT-1 was assessed semiquantitatively by the product of scores estimated (intensity × % positivity) according to our previous reports (*16,22*). The intensity of staining was graded (intensity) from 0 to 3 (0, not stained; 1, equivocal; 2, intense staining; and 3, very intense staining) and the percentage of positively stained cells (% positivity) was scored from 1 to 5 (1, 0%–20%; 2, 21%–40%; 3, 41%–60%; 4, 61%–80%; and 5, 81%–100%). The mean values of these levels were determined as immunohistologic GLUT-1 expression level.

Statistical Analysis

All values are shown as mean ± SD. Statistical analyses were performed using an unpaired Student *t* test to evaluate the significance of differences in values between the control and treated rats (*7,10*). Simple regression analysis was performed to compare the uptake of ^{99m}Tc-annexin V and that of ^{18}F-FDG. A 2-tailed value of $P < 0.05$ was considered significant.

RESULTS

Determination of Apoptosis

The uptake of ^{99m}Tc-annexin V in tumor tissue after gemcitabine and cyclophosphamide treatment was 0.062 ± 0.012 and 0.050 ± 0.012 (%ID/g) × kg, respectively (Table 1). The uptake of ^{99m}Tc-annexin V in tumor in both treated groups was significantly higher than that in the control group (0.031 ± 0.005 (%ID/g) × kg; $P < 0.01$). Two of the radiopharmaceuticals' uptakes in blood and muscle were not altered significantly by the 2 kinds of chemotherapeutic treatments. The TBRs of ^{99m}Tc-annexin V were 2.021 ± 0.323, 2.482 ± 0.407, and 1.414 ± 0.082 and the TMRs of ^{99m}Tc-annexin V were 7.283 ± 1.632, 7.095 ± 1.328, and 4.497 ± 0.824 in the gemcitabine-treated, cyclophosphamide-treated, and control groups, respectively. Both TBR and TMR in the treated groups were also significantly higher than those in the control group ($P < 0.01$).

In the gemcitabine-treated, cyclophosphamide-treated, and control groups, the rate of TUNEL positively stained cells were 10.2% ± 1.7%, 8.0% ± 1.5%, and 5.2% ± 1.5%, respectively. These apoptotic rates also increased in both treatment groups (Table 1).

Determination of Glucose Utilization

The uptake of ^{18}F-FDG in tumor tissue after gemcitabine and cyclophosphamide treatment was 0.483 ± 0.118 and 0.583 ± 0.142 (%ID/g) × kg, respectively (Table 2). The uptake of ^{18}F-FDG in tumor in both treated groups was significantly lower than that in the control group (0.743 ± 0.084 (%ID/g) × kg; $P < 0.01$). The TBRs of ^{18}F-FDG were 9.885 ± 4.592, 12.21 ± 7.145, and 15.21 ± 1.487 and the TMRs of ^{18}F-FDG were 15.15 ± 6.062, 7.859 ± 4.464, and 33.44 ± 4.721 in the gemcitabine-treated, cyclophosphamide-treated, and control groups, respectively. Both the TBRs and TMRs in the treated groups were also significantly lower than those in the control group ($P < 0.05$).

The expression levels of GLUT-1 estimated on the basis of positivity (intensity × percentage) were 58.3 ± 4.9, 61.1 ± 6.9, and 60.5 ± 5.6 in the gemcitabine-treated, cyclophosphamide-treated, and control groups, respectively. Although all 3 groups showed very high expression levels in the cancer cells, there was no statistically significant difference in the expression level of GLUT-1 between treated and control tissues (Table 2).

Relationship Between Uptake of ^{99m}Tc-Annexin V and ^{18}F-FDG in Tumor

Figure 2 shows a scattergram of the uptake of ^{99m}Tc-annexin V and ^{18}F-FDG in tumor. ^{18}F-FDG uptake in tumor showed a significantly negative correlation with that of ^{99m}Tc-annexin V uptake ($r = -0.75$; $P < 0.01$).

Blood Glucose Level and Tumor Weight

The tumor weights were 3.239 ± 1.520, 4.168 ± 2.007, and 3.503 ± 1.145 g in the gemcitabine-treated, cyclophosphamide-treated, and control groups, respectively. The blood glucose levels at BS1 was 114.1 ± 13.01, 118.9 ±

TABLE 1
Apoptotic Indices According to Uptake of ^{99m}Tc-Annexin V and Rate of TUNEL Positively Stained Cells

Parameter	Control	Gemcitabine	Cyclophosphamide
Tumor uptake (%ID/g) × kg	0.031 ± 0.005	0.062 ± 0.012*	0.050 ± 0.012*
Blood uptake (%ID/g) × kg	0.022 ± 0.002	0.024 ± 0.004*	0.025 ± 0.004*
Muscle uptake (%ID/g) × kg	0.007 ± 0.002	0.007 ± 0.003*	0.009 ± 0.002*
T/B ratio	1.414 ± 0.082	2.021 ± 0.323*	2.482 ± 0.407*
T/M ratio	4.497 ± 0.824	7.283 ± 1.632*	7.095 ± 1.328*
TUNEL positive (%)	5.2 ± 1.5	10.2 ± 1.7*	8.0 ± 1.5*

*$P < 0.01$ compared with control group.
Data are mean ± SD.

TABLE 2
Tumor Glucose Metabolic Markers According to Uptake of ^{18}F-FDG and Index of GLUT-1 Positivity

Parameter	Control	Gemcitabine	Cyclophosphamide
Tumor uptake (%ID/g) × kg	0.743 ± 0.084	0.483 ± 0.118*	0.583 ± 0.142*
Blood uptake (%ID/g) × kg	0.048 ± 0.005	0.045 ± 0.011*	0.036 ± 0.007*
Muscle uptake (%ID/g) × kg	0.022 ± 0.002	0.021 ± 0.004*	0.026 ± 0.006*
T/B ratio	15.21 ± 1.487	9.885 ± 4.592*	12.21 ± 7.145*
T/M ratio	33.44 ± 4.721	15.15 ± 6.062*	7.859 ± 4.464*
GLUT-1 (intensity × %)	60.5 ± 5.6	58.3 ± 4.9	61.1 ± 6.9

*$P < 0.01$ compared with control group.
Data are mean ± SD.

12.29, and 117.3 ± 5.283 mg/dL and those at BS2 were 93.86 ± 13.45, 94.14 ± 14.70, and 91.86 ± 14.86 mg/dL in the gemcitabine-treated, cyclophosphamide-treated, and control groups, respectively. Both tumor weight and blood glucose level in all groups did not change significantly after chemotherapeutic treatment with gemcitabine and cyclophosphamide (Table 3).

DISCUSSION

This study demonstrated that tumor glucose utilization declined after a single dose of gemcitabine or cyclophosphamide, which was not based on reduced GLUT-1 expression. This decline in glucose utilization occurred at a time of increased apoptosis. These molecular events occurred before the actual tumor regression. These data suggest that apoptosis induced by chemotherapy is not always accompanied by glucose hypermetabolism for survival reactions as previously reported (*17,23*).

In clinical oncology, the decrease in ^{18}F-FDG uptake was usually associated with a good lesion response, especially in malignant lymphoma, esophageal cancer, and head and neck cancer (*13,14*). Recently, there have been reports that

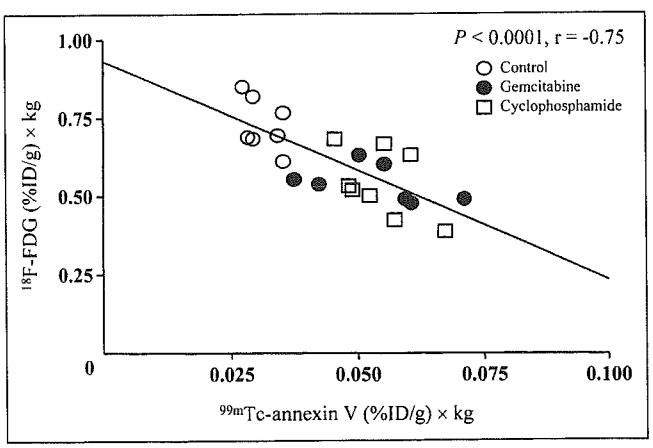

FIGURE 2. Negative correlation between ^{18}F-FDG uptake and ^{99m}Tc-annexin V uptake in control, gemcitabine-treated, and cyclophosphamide-treated groups. ^{18}F-FDG uptake ((%ID/g) × kg) = 0.932 − (6.956 ^{99m}Tc-annexin V uptake ((%ID/g) × kg)) ($r = -0.75$; $P < 0.01$).

^{99m}Tc-annexin V is very useful for detecting and in vivo imaging of apoptosis (*4,24,25*). The present study demonstrated that induction of apoptosis with a single dose of chemotherapy was associated with a striking reduction in ^{18}F-FDG uptake and a modest increase in annexin localization. Although appropriate chemotherapy induces metabolic regression (reflected by a reduction in ^{18}F-FDG uptake) before morphologic change of cancer tissue, the basic mechanism underlying the decrease in glucose uptake is not well understood. We observed that the uptake of ^{18}F-FDG was definitely decreased to approximately 55% of the control value by both gemcitabine and cyclophosphamide before the actual tumor regression. Both gemcitabine and cyclophosphamide themselves rarely affected blood glucose level, and our present results confirmed this observation. Mazurek et al. (*26,27*) suggested the following mechanisms: Chemotherapeutic agents damage DNA and then they activate adenosine diphosphate ribosyl transferase to repair DNA for proliferation. Because this repair requires a great amount of energy, intracellular nicotinamide adenine dinucleotide, which is an electron carrier, and adenosine triphosphate, which is required in intracellular phosphorylation, are so exhausted by anaerobic hyperglycolysis, they cannot compensate. This intracellular "famine" may depress important glycolytic enzymes. Consequently, glucose uptake in cancer cells decreases as a result of these intracellular reactions.

The relationship between apoptosis and glucose utilization at the early stage of cancer chemotherapy is also controversial (*17,28*). Haberkorn et al. reported an increase in glucose (^{18}F-FDG) uptake early after chemotherapy using gemcitabine for Morris hepatoma and interpreted it as a stress reaction of cancer cells as a protective mechanism against apoptosis (*17*). This interpretation may be reasonable since a great amount of energy is required for DNA repair. Furthermore, DNA damage promotes apoptosis via other pathways, such as the activation of tumor-suppression gene (e.g., p53) and inhibition of antiapoptotic molecules (e.g., Fas and phosphatidylinositol 3-phosphate kinase (PI3K-Akt)) (*29–32*). Activated caspases also have an essential role in the series of apoptosis. As a result of these

TABLE 3
Blood Glucose Level and Weight of Whole Body and Tumor

Parameter	Control	Gemcitabine	Cyclophosphamide	*P*
BS1 (mg/dL)	117.3 ± 5.283	114.1 ± 13.01	118.9 ± 12.29	ns
BS2 (mg/dL)	91.86 ± 14.86	93.86 ± 13.45	94.14 ± 14.70	ns
Whole-body weight (g)	209.6 ± 14.59	215.4 ± 14.29	204.9 ± 14.86	ns
Tumor weight (g)	3.503 ± 1.145	3.239 ± 1.520	4.168 ± 2.007	ns

ns = not significant.
Data are mean ± SD.

molecular interactions, an irreversible DNA-laddering reaction occurs at the end of programmed cell death. Because this reaction must use energy, glucose demand may increase temporarily. Occasionally, a "metabolic flare" was often observed on ^{18}F-FDG PET images after hormonal therapy was administrated for estrogen receptor–positive human breast cancer. This phenomenon may indicate responsiveness (*33*). Here, we speculated that tumor glucose hypometabolism was finally superior to the energy demand. Previous studies demonstrated maximal apoptosis 1 or 2 d after chemotherapy (*7,10,34*). Although ATP depletion and decrease in glucose uptake occur as apoptosis progresses after chemotherapy, these 2 phenomena themselves were reported to promote apoptosis (*26,35*). Thus, we confidently assumed that tumor glucose utilization after chemotherapy increasingly becomes hypometabolic and, finally, irreversible. Additionally, Spaepen et al. suggested that FDG uptake mainly correlates with the viable tumor cell fraction for 15-d monitoring of tumor response using a leukemia model in mice with severe combined immunodeficiency (*36*). However, changes in glucose metabolism by chemotherapy still remain to be clarified. Correlation between tumor uptake of ^{18}F-FDG and ^{99m}Tc-annexin V may help clarify the significance of early glucose utilization changes in clinical oncology. A long-time course of chemotherapeutic effects should also be evaluated in vivo models. Cremerius et al. reported FDG PET must be performed 2 wk after completion of therapy of metastatic germ cell tumor (*37*). Until the various histologic changes that influence glucose utilization become inactive, a high accuracy of FDG PET evaluation cannot be maintained. The serial ^{18}F-FDG and ^{99m}Tc-annexin V images each provide useful data for predicting a therapeutic response.

In this study, we investigated whether GLUT-1 expression affects tumor glucose utilization. However, GLUT-1 protein expression level did not change significantly after chemotherapy in our immunohistologic analyses. Histologic GLUT-1 overexpression correlated significantly with tumor characterization and prognosis in many cancer tissues. If ^{18}F-FDG uptake is high, GLUT-1 expression level also tends to be high. These findings are usually seen more with malignant lesions (*38*). In the present study, GLUT-1 expression was evaluated with "percent positive" and "intensity" per randomly selected high-power microscopic field. However, changes in cellularity by chemotherapy may affect the values of GLUT-1 expression rate if it is normalized to the cell number. Further evaluation considering the cellularity is needed to confirm the present results, although no apparent difference in the cell numbers (approximately 1,000 cells per field) was observed among the 3 groups. Unfortunately, little was known in our study as to why GLUT-1 positivity was not seemingly altered by chemotherapy. Using MR spectroscopy and western blotting, Rivenzon-Segal et al. suggested that glycolysis and GLUT-1 expression in breast tumor cells were positively correlated at both estrogen stimulation and tamoxifen inhibition (*39*). We deduce 2 points: (a) GLUT-1 protein expression is maintained for self-survival and (b) there is a time lag between the present protein expression on the cell surface and messenger RNA expression. Furthermore, this mechanism is more complicated because of the participation in hexokinase or the other GLUTs. Cyclophosphamide treatment was reported to modify tumor glycolytic rate and increase the intracellular lactate concentration in RIF-1 tumor (*40*).

In the present study, the animals were anesthetized with pentobarbital, which is known to depress glucose metabolism. This kind of barbiturate is a sedative-hypnotic drug, and its high lipophilicity has a direct effect on the central nervous system. The depressed glucose metabolism by pentobarbital may cause systemic errors. On the other hand, direct competition between FDG and blood glucose is regarded as the cause of impaired FDG uptake in tumors. Accordingly, we used anesthetized animals to avoid any physiologic variations, including blood glucose concentration, among the groups. It is also well known that blood glucose concentration is easily affected by any stress in awake animals.

The weakness of our study is the acute or chronic nature of our measurements. The animals received a single, high dose of chemotherapy to treat a rapidly growing tumor. The tumor response was evaluated within hours of chemotherapy administration. Whether serial administration of more moderate doses could produce a similar early result cannot be determined from the present study. However, there are clinical instances when an early indication of therapeutic

response is required. This is particularly necessary when toxic chemotherapy is used in tumors, such as gastric or lung cancer, where the response rate is around 50%. In those cases, an indication of nonresponse would permit a rapid redirection of therapy to other agents.

CONCLUSION

We found that the enhanced apoptotic reaction correlated with suppressed tumor glucose utilization after cytotoxic chemotherapy. The imaging results were confirmed by histologic evaluation. The decrease in tumor glucose utilization was independent of GLUT-1 overexpression. The increase in ^{99m}Tc-annexin V uptake in tumor as well as the decrease in ^{18}F-FDG uptake can be useful markers for predicting therapeutic outcomes and for prognosis at the early stage of chemotherapy.

ACKNOWLEDGMENTS

The authors are grateful to Professors Shinzo Nishi, Kazuo Miyasaka, and Koh-ichi Seki of the Central Institute of Isotope Science, Hokkaido University, for supporting this work. The authors also thank Koutaro Suzuki, Hidenori Katsuura, Hidehiko Omote, Hiroshi Arai, Keiichi Magota, and Miho Nakajima of the Facility of Radiology, Hokkaido University Medical Hospital, for assistance; Theseus Imaging Corp. for providing annexin V protein; and Makoto Sato, Sumitomo Heavy Industries, Ltd., for ^{18}F-FDG syntheses.

REFERENCES

1. Kerr JF, Wyllie AH, Currie AR. Apoptosis: a basic biological phenomenon with wide-ranging implications in tissue kinetics. *Br J Cancer.* 1972;26:239–257.
2. Thompson CB. Apoptosis in the pathogenesis and treatment of disease. *Science.* 1995;267:1456–1462.
3. Joseph B, Lewensohn R, Zhivotovsky B. Role of apoptosis in the response of lung carcinomas to anti-cancer treatment. *Ann NY Acad Sci.* 2000;926:204–216.
4. Belhocine T, Steinmetz N, Green A, Rigo P. In vivo imaging of chemotherapy-induced apoptosis in human cancers. *Ann NY Acad Sci.* 2003;1010:525–529.
5. Vermeersch H, Ham H, Rottey S, et al. Intraobserver, interobserver, and day-to-day reproducibility of quantitative ^{99m}Tc-HYNIC annexin-V imaging in head and neck carcinoma. *Cancer Biother Radiopharm.* 2004;19:205–210.
6. Ng SSW, Tsao MS, Chow S, Hedley DW. Inhibition of phosphatidylinositide 3-kinase enhances gemcitabine-induced apoptosis in human pancreatic cancer cells. *Cancer Res.* 2000;60:5451–5455.
7. Mochizuki T, Kuge Y, Zhao S, et al. Detection of apoptotic tumor response in vivo after a single dose of chemotherapy with ^{99m}Tc-annexin V. *J Nucl Med.* 2003;44:92–97.
8. Blankenberg FG, Katsikis PD, Tait JF, et al. In vivo detection and imaging of phosphatidylserine expression during programmed cell death. *Proc Natl Acad Sci USA.* 1998;95:6349–6354.
9. Kuge Y, Sato M, Zhao S, et al. Feasibility of ^{99m}Tc-annexin V for repetitive detection of apoptotic tumor response to chemotherapy: an experimental study using a rat tumor model. *J Nucl Med.* 2004;45:309–312.
10. Takei T, Kuge Y, Zhao S, et al. Time course of apoptotic tumor response following a single dose of chemotherapy: comparison with ^{99m}Tc-annexin V uptake and histologic findings in an experimental model. *J Nucl Med.* 2004;45:2083–2087.
11. Cohade C, Wahl RL. PET scanning and measuring the impact of treatment. *Cancer J.* 2002;8:119–134.
12. Rohren EM, Turkington TG, Coleman RE. Clinical applications of PET in oncology. *Radiology.* 2004;231:305–332.
13. Brun E, Kjellen E, Tennvall J, et al. FDG PET studies during treatment: prediction of therapy outcome in head and neck squamous cell carcinoma. *Head Neck.* 2002;24:127–135.
14. Spaepen K, Stroobants S, Verhoef G, Mortelmans L. Positron emission tomography with [^{18}F]FDG for therapy response monitoring in lymphoma patients. *Eur J Nucl Med Mol Imaging.* 2003;30(suppl 1):S97–S105.
15. Zhao S, Kuge Y, Tsukamoto E, et al. Effects of insulin and glucose loading on FDG uptake in experimental malignant tumours and inflammatory lesions. *Eur J Nucl Med.* 2001;28:730–735.
16. Mochizuki T, Tsukamoto E, Kuge Y, et al. FDG uptake and glucose transporter subtype expressions in experimental tumor and inflammation models. *J Nucl Med.* 2001;42:1551–1555.
17. Haberkorn U, Bellemann ME, Brix G, et al. Apoptosis and changes in glucose transport early after treatment of Morris hepatoma with gemcitabine. *Eur J Nucl Med.* 2001;28:418–425.
18. Wood BL, Gibson DF, Tait JF. Increased erythrocyte phosphatidylserine exposure in sickle cell disease: flow-cytometric measurement and clinical associations. *Blood.* 1996;88:1873–1880.
19. Tait JF, Smith C. Site-specific mutagenesis of annexin V: role of residues from Arg-200 to Lys-207 in phospholipid binding. *Arch Biochem Biophys.* 1991;288:141–144.
20. Tait JF, Engelhardt S, Smith C, Fujikawa K. Prourokinase-annexin V chimeras: construction, expression, and characterization of recombinant proteins. *J Biol Chem.* 1995;270:21594–21599.
21. Tait JF, Brown DS, Gibson DF, Blankenberg FG, Strauss HW. Development and characterization of annexin V mutants with endogenous chelation sites for ^{99m}Tc. *Bioconjug Chem.* 2000;11:918–925.
22. Zhao S, Kuge Y, Tsukamoto E, et al. Fluorodeoxyglucose uptake and glucose transporter expression in experimental inflammatory lesions and malignant tumours: effects of insulin and glucose loading. *Nucl Med Commun.* 2002;23:545–550.
23. Haberkorn U, Bellemann ME, Altmann A, et al. PET 2-fluoro-2-deoxyglucose uptake in rat prostate adenocarcinoma during chemotherapy with gemcitabine. *J Nucl Med.* 1997;38:1215–1221.
24. Belhocine T, Steinmetz N, Hustinx R, et al. Increased uptake of the apoptosis-imaging agent ^{99m}Tc recombinant human annexin V in human tumors after one course of chemotherapy as a predictor of tumor response and patient prognosis. *Clin Cancer Res.* 2002;8:2766–2774.
25. van de Wiele C, Lahorte C, Vermeersch H, et al. Quantitative tumor apoptosis imaging using technetium-99m-HYNIC annexin V single photon emission computed tomography. *J Clin Oncol.* 2003;21:3483–3487.
26. Mazurek S, Boschek CB, Eigenbrodt E. The role of phosphometabolites in cell proliferation, energy metabolism, and tumor therapy. *J Bioenerg Biomembr.* 1997;29:315–330.
27. Mazurek S, Eigenbrodt E. The tumor metabolome. *Anticancer Res.* 2003;23:1149–1154.
28. Moley KH, Mueckler MM. Glucose transport and apoptosis. *Apoptosis.* 2000;5:99–105.
29. Fresno Vara JA, Casado E, de Castro J, et al. PI3K/Akt signalling pathway and cancer. *Cancer Treat Rev.* 2004;30:193–204.
30. Raff M. Cell suicide for beginners. *Nature.* 1998;396:119–122.
31. Thorburn A, Thorburn J, Frankel AE. Induction of apoptosis by tumor cell-targeted toxins. *Apoptosis.* 2004;9:19–25.
32. Sellers WR, Fisher DE. Apoptosis and cancer drug targeting. *J Clin Invest.* 1999;104:1655–1661.
33. Mortimer JE, Dehdashti F, Siegel BA, et al. Metabolic flare: indicator of hormone responsiveness in advanced breast cancer. *J Clin Oncol.* 2001;19:2797–2803.
34. Blankenberg FG, Naumovski L, Tait JF, Post AM, Strauss HW. Imaging cyclophosphamide-induced intramedullary apoptosis in rats using ^{99m}Tc-radiolabeled annexin V. *J Nucl Med.* 2001;42:309–316.
35. Bacurau RF, O'Toole CE, Newsholme P, Costa Rosa LF. Sub-lethal concentrations of activated complement increase rat lymphocyte glutamine utilization and oxidation while lethal concentrations cause death by a mechanism involving ATP depletion. *Cell Biochem Funct.* 2002;20:183–190.
36. Spaepen K, Stroobants S, Dupont P, et al. [^{18}F]FDG PET monitoring of tumour response to chemotherapy: does [^{18}F]FDG uptake correlate with the viable tumour cell fraction? *Eur J Nucl Med Mol Imaging.* 2003;30:682–688.
37. Cremerius U, Effert PJ, Adam G, et al. FDG PET for detection and therapy control of metastatic germ cell tumor. *J Nucl Med.* 1998;39:815–822.
38. Medina RA, Owen GI. Glucose transporters: expression, regulation and cancer. *Biol Res.* 2002;35:9–26.
39. Rivenzon-Segal D, Boldin-Adamsky S, Seger D, Seger R, Degani H. Glycolysis and glucose transporter 1 as markers of response to hormonal therapy in breast cancer. *Int J Cancer.* 2003;107:177–182.
40. Poptani H, Bansal N, Jenkins WT, et al. Cyclophosphamide treatment modifies tumor oxygenation and glycolytic rates of RIF-1 tumors: ^{13}C magnetic resonance spectroscopy, Eppendorf electrode, and redox scanning. *Cancer Res.* 2003;63:8813–8820.

Biologic Correlates of Intratumoral Heterogeneity in ^{18}F-FDG Distribution with Regional Expression of Glucose Transporters and Hexokinase-II in Experimental Tumor

Songji Zhao, MD[1,2]; Yuji Kuge, PhD[2]; Takafumi Mochizuki, MD[3]; Toshiyuki Takahashi, MD[4]; Kunihiro Nakada, MD[1]; Masayuki Sato, BS[1]; Toshiki Takei, MD[1]; and Nagara Tamaki, MD[1]

[1]Department of Nuclear Medicine, Graduate School of Medicine, Hokkaido University, Sapporo, Japan; [2]Department of Tracer Kinetics, Graduate School of Medicine, Hokkaido University, Sapporo, Japan; [3]Department of Radiology, Nikko Memorial Hospital, Muroran, Japan; and [4]Department of Pathology, Hokkaido Gastroenterology Hospital, Sapporo, Japan

The biologic mechanisms involved in the intratumoral heterogeneous distribution of ^{18}F-FDG have not been fully investigated. To clarify factors inducing heterogeneous ^{18}F-FDG distribution, we determined the intratumoral distribution of ^{18}F-FDG by autoradiography (ARG) and compared it with the regional expression levels of glucose transporters Glut-1 and Glut-3 and hexokinase-II (HK-II) in a rat model of malignant tumor. **Methods:** Rats were inoculated with allogenic hepatoma cells (KDH-8) into the left calf muscle ($n = 7$). Tumor tissues were excised 1 h after the intravenous injection of ^{18}F-FDG and sectioned to obtain 2 adjacent slices for ARG and histochemical studies. The regions of interest (ROIs) were placed on ARG images to cover mainly the central (CT) and peripheral (PT) regions of viable tumor tissues and necrotic/apoptotic (NA) regions. The radioactivity in each ROI was analyzed quantitatively using a computerized imaging analysis system. The expression levels of Glut-1, Glut-3, and HK-II were determined by immunostaining and semiquantitative evaluation. The hypoxia-inducible factor 1α (HIF-1α) was also immunostained. **Results:** ARG images showed that intratumoral ^{18}F-FDG distribution was heterogeneous. The accumulation of ^{18}F-FDG in the CT region was the highest, which was 1.6 and 2.3 times higher than those in the PT and NA regions, respectively ($P < 0.001$). The expression levels of Glut-1, Glut-3, and HK-II were markedly higher in the CT region ($P < 0.001$) compared with those in the PT region. The intratumoral distribution of ^{18}F-FDG significantly correlated with the expression levels of Glut-1, Glut-3, and HK-II ($r = 0.923$, $P < 0.001$ for Glut-1; $r = 0.829$, $P < 0.001$ for Glut-3; and $r = 0.764$, $P < 0.01$ for HK-II). The positive staining of HIF-1α was observed in the CT region. **Conclusion:** These results demonstrate that intratumoral ^{18}F-FDG distribution corresponds well to the expression levels of Glut-1, Glut-3, and HK-II. The elevated expression levels of Glut-1, Glut-3, and HK-II, induced by hypoxia (HIF-1α), may be contributing factors to the higher ^{18}F-FDG accumulation in the CT region.

Key Words: ^{18}F-FDG; glucose transporters; hexokinase; heterogeneity; tumor

J Nucl Med 2005; 46:675–682

PET using ^{18}F-FDG has been widely used not only for detecting and staging malignant tumors but also for monitoring therapy response and for differentiating malignant lesions from benign lesions (*1–4*). These applications are based on the increased ^{18}F-FDG uptake due to enhanced glucose utilization in most tumors. The increased ^{18}F-FDG accumulation in malignant tumors is associated with the rate of transport across the cell membrane, the activity of hexokinase, and the rate of dephosphorylation in the tissue (*5,6*). The transport of ^{18}F-FDG across cell membranes is mediated by ≥5 structurally related proteins (constituting a family of glucose transporters, Glut-1 to Glut-5) (*7,8*). Significantly elevated expression levels of Glut-1 and Glut-3 are considered to be a factor contributing to the accumulation of ^{18}F-FDG in malignant tumors (*9–13*). It has also been suggested that the activity level of hexokinase-II (HK-II) contributes to ^{18}F-FDG accumulation in various malignant tumors (*14*). These studies, however, used PET or tissue-counting techniques and correlated average ^{18}F-FDG accumulation in the tumor with protein expression.

It is well known that various components, including nonmalignant components, are involved in most solid tumors (*15–17*). Tumor tissues also show intratumoral heterogeneity in their various properties, which may originate from the diverse phenotypic properties of tumor cells or may be induced by their metabolic microenvironment (*18–20*). In this regard, intratumoral heterogeneity in ^{18}F-FDG distribution has been well demonstrated by autoradiography (ARG)

Received Sep. 3, 2004; revision accepted Nov. 23, 2004.

For correspondence or reprints contact: Nagara Tamaki, MD, Department of Nuclear Medicine, Graduate School of Medicine, Hokkaido University, Kita 15 Nishi 7, Kita-ku, Sapporo 060-8638, Japan.

E-mail: natamaki@med.hokudai.ac.jp

(*15*). However, there have been few reports regarding the biologic mechanisms involved in the intratumoral heterogeneous distribution of ^{18}F-FDG. The relationships between the intratumoral distribution of ^{18}F-FDG and the regional expression of glucose transporters or hexokinases remain to be investigated. Such data should be helpful in understanding the mechanism of ^{18}F-FDG uptake in malignant tumors and should provide the biologic basis for diagnosing, staging, and prognosticating malignant tumors and monitoring therapy response by ^{18}F-FDG PET.

To clarify factors inducing heterogeneous ^{18}F-FDG distribution, we determined in this study the intratumoral distribution of ^{18}F-FDG by ARG and compared it with the regional expression levels of Glut-1, Glut-3, and HK-II in a rat model of malignant tumor.

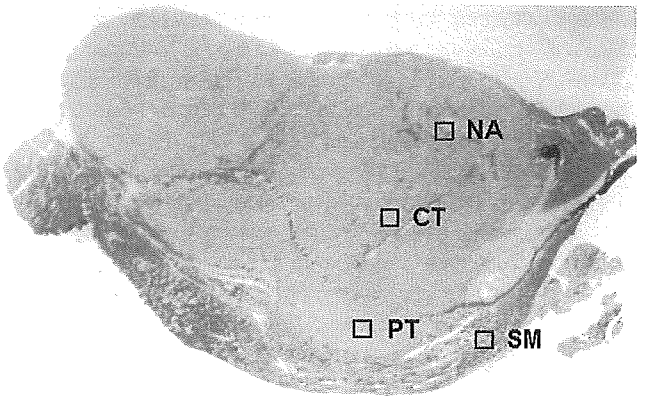

FIGURE 1. ROIs were placed on ARG image, to cover mainly central (CT) and peripheral (PT) regions of viable tumor tissues and necrotic/apoptotic (NA) regions, with reference to corresponding sections stained with HE. SM = surrounding muscle.

MATERIALS AND METHODS

Animal Studies

The experimental protocol was completely approved by the Laboratory Animal Care and Use Committee of Hokkaido University. Male Wistar King Aptekman/hok (WKAH) rats, weighing 203–268 g, were inoculated with a suspension of allogenic hepatoma cells (KDH-8, 1×10^6 cells per rat) into the left calf muscle. Two weeks after the tumor inoculation, when the tumors were 2–3 cm in diameter, the rats were fasted overnight ($n = 7$) (*21*). Each rat was anesthetized with pentobarbital (50 mg/kg body weight, intraperitoneally) and was injected in the tail vein with 37 MBq of ^{18}F-FDG synthesized as previously described (*22*). Sixty minutes after the ^{18}F-FDG injection, the animals were sacrificed and the tumors were quickly excised. Each tumor tissue was then sectioned at 2- to 3-mm thickness to obtain 2 adjacent slices. One of the 2 slices was embedded in Tissue-Tek medium (Sakura Finetechnical Co., Ltd.) and frozen in isopentane/dry ice for ARG studies. Formalin-fixed, paraffin-embedded specimens were prepared using the other slice for subsequent histochemical studies (*23*).

ARG Studies

The frozen samples were cut into 20-μm sections with a CM3050-Cryostat (Leica) at −20°C. The tumor sections were placed in a phosphor image plate cassette, together with a set of calibrated standards (*17*), and an overnight ARG exposure was used to detect the distribution of ^{18}F-FDG. The tumor sections (10 μm) adjacent to those used for the ARG studies were stained with hematoxylin and eosin (HE) for use as the reference to determine the regions of interest (ROIs) on the autoradiograms.

The ARG images were analyzed using a computerized imaging analysis system (BAS 5000 Bio-Imaging Analyzer; Fuji Photo Film Co., Ltd.). The resolution of ARG of the BAS 5000 is 100 μm. To quantitatively evaluate the distribution of ^{18}F-FDG radioactivity, 32 ROIs (0.36 mm^2) were determined on each ARG image. ROIs were placed to cover mainly the central (CT; $n = 8$) and peripheral (PT; $n = 8$) regions of the viable tumor tissues, necrotic/apoptotic (NA; $n = 8$) regions, and the surrounding muscle (SM; $n = 8$), by referring to the sections stained with HE (Fig. 1); each ROI was selected microscopically by a pathologist and identified by its predominant histologic characteristic as a region of the viable tumor cells and necrotic/apoptotic cells in the CT and PT regions on the HE section. Large necrotic regions occasionally observed in the center of the tumors were excluded from the evaluation. To avoid any bias, these ROIs were determined in a blind manner for ARG images and immunologic staining (Gluts and HK-II). The ROIs placed on HE images were transferred to ARG images by using computer software (MCID-M2 Image Analyzer; Imaging Research Inc.). Briefly, coordinates were set on both HE and ARG images, the coordinates of each ROI on the HE images was determined, and then each ROI was transferred to the same coordinates of the corresponding ARG images. The radioactivity in each ROI was shown by photostimulated luminescence per unit area, PSL/mm^2 ($PSL = a \cdot D \cdot t$: a = constant; D = radioactivity exposed on imaging plate; t = exposed time); then each count of PSL/mm^2 from a tumor section was recorded and used to calculate the mean counts per mm^2 and converted to the percentage injected dose per gram (%ID/g) of tissue by using activity of the standards, with the assumption that tissue density is 1 g/cm^3 (*17,24*). The mean radioactivities of the 8 ROIs determined for the CT, PT, NA regions, and SM, respectively, were used to evaluate the ^{18}F-FDG accumulation in the tissues.

Histochemical Studies

The expression of Glut-1, Glut-3, and HK-II was studied in the sections of a formalin-fixed, paraffin-embedded tumor according to a standard immunostaining procedure (*10,25*). Briefly, after deparaffization and rehydration, endogenous peroxidase activity was blocked for 10 min in methanol containing 3% hydrogen peroxide. Thereafter, endogenous nonspecific antigens were blocked in 10% normal goat albumin (HISTOFINE SAB-PO kit; Nichirei) for 10 min at 37°C and then incubated with an anti-Glut-1, anti-Glut-3, or antihexokinase II antibody (Chemicon International Inc.) for 30 min at 37°C. The bound antibody was visualized using the avidin/biotin conjugate immunoperoxidase procedure (ABC) with the HISTOFINE SAB-PO kit and 3,3′-diaminobenzidine tetrahydrochloride. Tumor sections adjacent to those used for these histochemical studies were also stained with anti-HIF-1α (mouse antihypoxia-inducible factor 1α monoclonal IgG 2b, clone H1α67; Novus Biologicals) using the method of Zhong et al. (*26*) with slight modification. Briefly, after deparaffinization and rehydration, the slides were initially immersed in a target retrieval solution (10 mmol/L ethylenediaminetetraacetic acid, pH 8.0) and heated in a microwave oven (500 W) for 20 min.

After the antigen retrieval, endogenous peroxidase activity was blocked for 5 min in methanol containing 3% hydrogen peroxide. Thereafter, endogenous nonspecific antigens were blocked in 10% hog albumin (Cosmo Bio., Ltd.) for 10 min and then incubated overnight with the primary antibody at 4°C. Finally, the bound antibody was visualized using the ABC procedure with the HISTOFINE MAX-PO (M) kit (Nichirei) and 3,3′-diaminobenzidine tetrahydrochloride. Tumor sections adjacent to those used for the immunostaining were stained with HE.

For immunohistochemical grading, ROIs placed on the HE-stained sections were transferred to immunologically stained sections as described. The intensity of staining and the percentage of positively stained cells in the CT (n = 8) and PT (n = 8) regions of the viable tumor tissues were evaluated microscopically. The intensity of staining (intensity) was graded from 0 to 3 (0 = not stained, 1 = equivocal, 2 = intense, and 3 = very intense) according to the criteria of Higashi et al. (*27*). Moreover, the percentage of positively stained cells (% positive) was classified from 1 to 5 (1 = 0%–20%, 2 = 20%–40%, 3 = 40%–60%, 4 = 60%–80%, and 5 = 80%–100%). The expression levels of Gluts and HK-II were assessed semiquantitatively using the product of these scores (intensity × % positive) (*28*). In HIF-1α staining, cells with completely and darkly stained nuclei were regarded as positively stained cells (*29*).

Statistical Analysis

All values are expressed as mean ± SD. One-way ANOVA and the Bonferroni post hoc test were used to assess the significance of differences due to the intratumoral distribution of ^{18}F-FDG. To evaluate the significance of differences in the expression levels of Glut-1, Glut-3, and HK-II (intensity × % positive) between the CT and PT regions, an unpaired Student t test was performed. Simple regression analysis was used to compare the intratumoral ^{18}F-FDG distribution and the expression levels of Glut-1, Glut-3, and HK-II. A 2-tailed P value < 0.05 was considered significant.

RESULTS

Intratumoral Distribution of ^{18}F-FDG

Figure 2A shows the representative autoradiogram of ^{18}F-FDG distribution in the tumor. The ARG images showed heterogeneous ^{18}F-FDG distribution with a relatively higher ^{18}F-FDG accumulation level in the CT regions of viable tumor tissues.

Results from the quantitative evaluation of ^{18}F-FDG distribution are summarized in Figure 2B. The accumulation of ^{18}F-FDG in the CT region was the highest (4.43 ± 0.50 %ID/g), which was 1.6 and 2.3 times higher than those in the PT region (2.85 ± 0.22 %ID/g) and the NA region (1.94 ± 0.10 %ID/g), respectively (P < 0.001). The accumulation of ^{18}F-FDG in the PT region was 1.5 times and was significantly higher than that in the NA region (P < 0.001). The distribution of ^{18}F-FDG in the SM (0.18 ± 0.01 %ID/g) was lower than those in any other ROIs determined in the tumor tissues (CT, PT, and NA).

Immunohistochemical Staining

The typical immunostaining of Glut-1, Glut-3, and HK-II in the CT and PT region is shown in Figure 3. The intensity and extent of staining of Glut-1, Glut-3, and HK-II were markedly higher in the CT region than those in the PT region.

The results of immunohistochemical grading are summarized in Figure 4. The histochemical grading scores for Glut-1 and Glut-3 were significantly higher in the CT region (11.34 ± 1.78 for Glut-1 and 6.02 ± 1.83 for Glut-3) than those in the PT region (4.23 ± 0.85 for Glut-1 and 2.29 ± 0.62 for Glut-3; P < 0.001 for both). The histochemical grading score for HK-II was also significantly higher in the

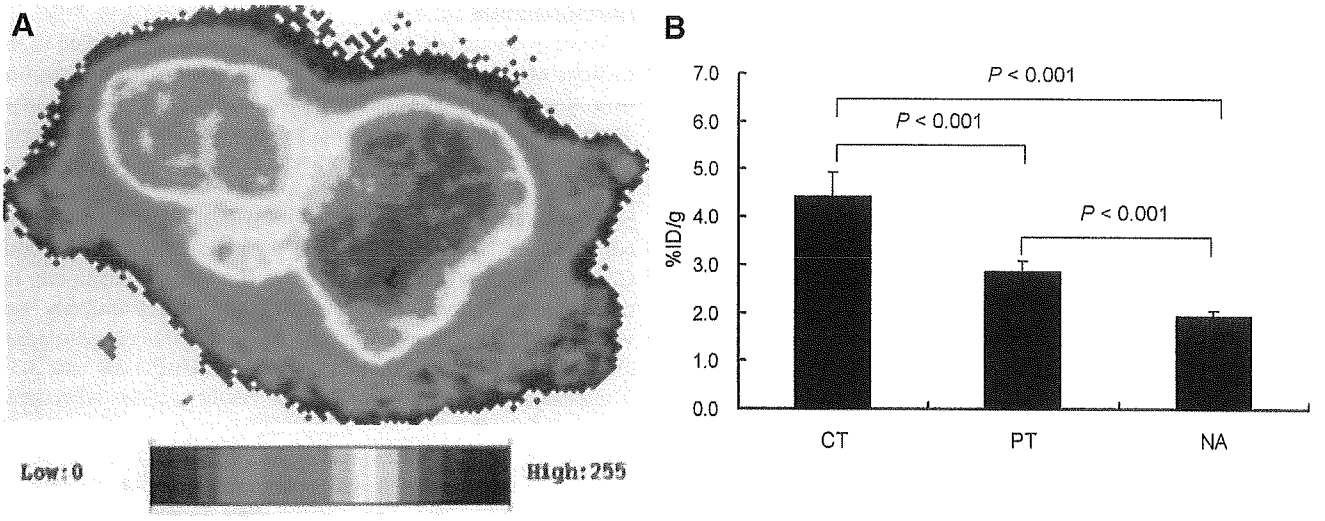

FIGURE 2. (A) Representative autoradiograph of ^{18}F-FDG distribution. ARG image shows intratumoral heterogeneous ^{18}F-FDG distribution. (B) Quantitative evaluation of intratumoral ^{18}F-FDG distribution. ^{18}F-FDG accumulation level in CT region was highest, which was 1.6 and 2.3 times higher than those in PT and NA regions, respectively (P < 0.001).

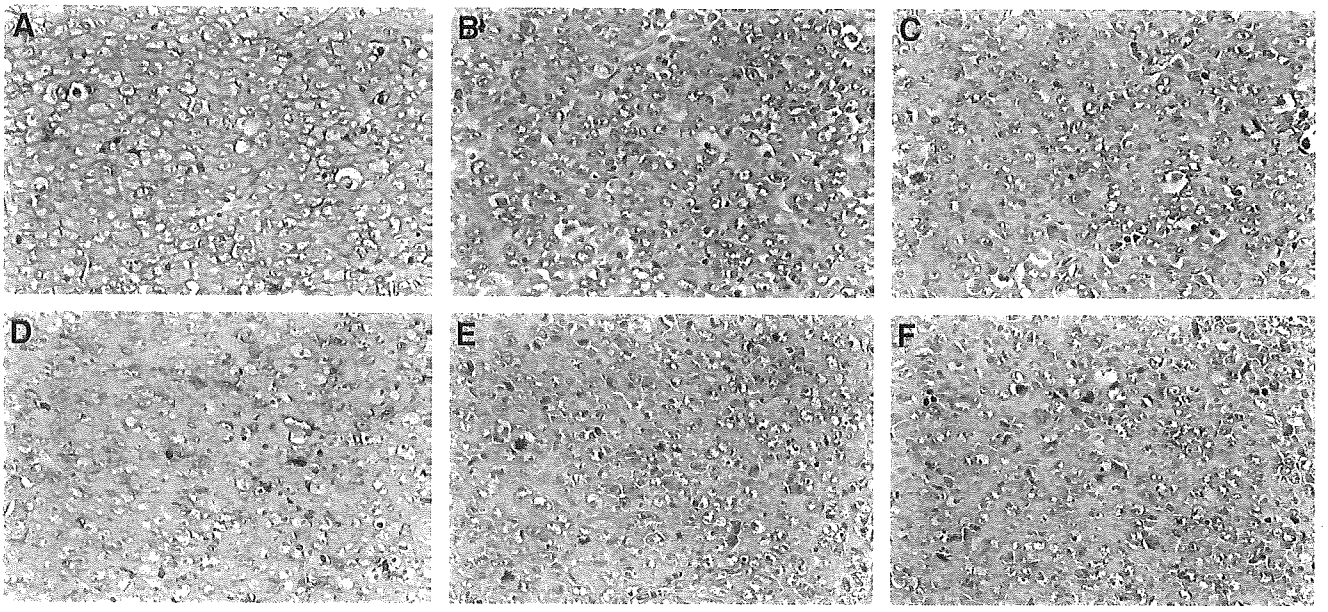

FIGURE 3. Staining with anti-Glut-1 (A and D), anti-Glut-3 (B and E), and anti-HK-II (C and F) antibodies in CT region (top) was more prominent than those in PT region (bottom) in KDH-8 tumor tissues, respectively (×400).

CT region (4.25 ± 0.98) compared with that in the PT region (2.00 ± 0.28; $P < 0.001$). The positive staining of HIF-1α was clearly observed in the CT region (Fig. 5) but not in the PT region.

Relationships Between ^{18}F-FDG Accumulation and Expression Levels of Gluts and HK-II

The accumulation of ^{18}F-FDG and the expression levels of Glut-1, Glut-3, and HK-II were significantly higher in the CT region than those in the PT region (Figs. 2 and 4). Figure 6 shows scattergrams of histochemical grading scores and ^{18}F-FDG accumulation. Intratumoral ^{18}F-FDG accumulation significantly correlated with the expression levels of Glut-1, Glut-3, and HK-II: $r = 0.923$, $P < 0.001$ for Glut-1; $r = 0.829$, $P < 0.001$ for Glut-3; and $r = 0.764$, $P < 0.01$ for HK-II.

DISCUSSION

In this study, a relatively higher ^{18}F-FDG accumulation was observed in the CT regions, with elevated expression levels of Glut-1, Glut-3, and HK-II. Positive staining of HIF-1α was observed in these regions. Intratumoral ^{18}F-FDG distribution significantly correlated with the expression levels of Glut-1, Glut-3, and HK-II. Consequently, the regional expression levels of Glut-1, Glut-3, and HK-II may increase in a hypoxic environment within tumor tissues and may contribute to heterogeneous ^{18}F-FDG distribution in the tumor tissues.

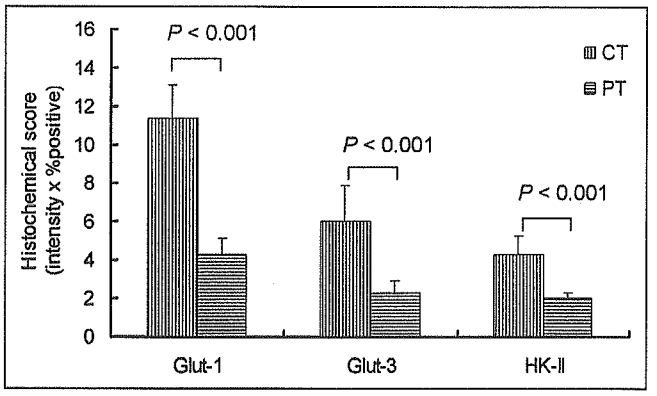

FIGURE 4. Expression levels of Glut-1, Glut-3, and HK-II were assessed by semiquantitative immunohistochemical grading performed by calculating the product of these scores (intensity × % positive). Histochemical scores of Glut-1, Glut-3, and HK-II were significantly higher in CT region than those in PT region ($P < 0.001$).

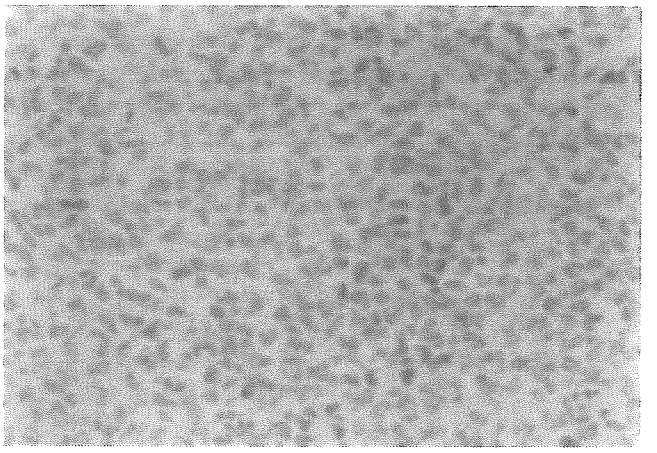

FIGURE 5. Positive staining of HIF-1α was clearly observed in CT region (×400).

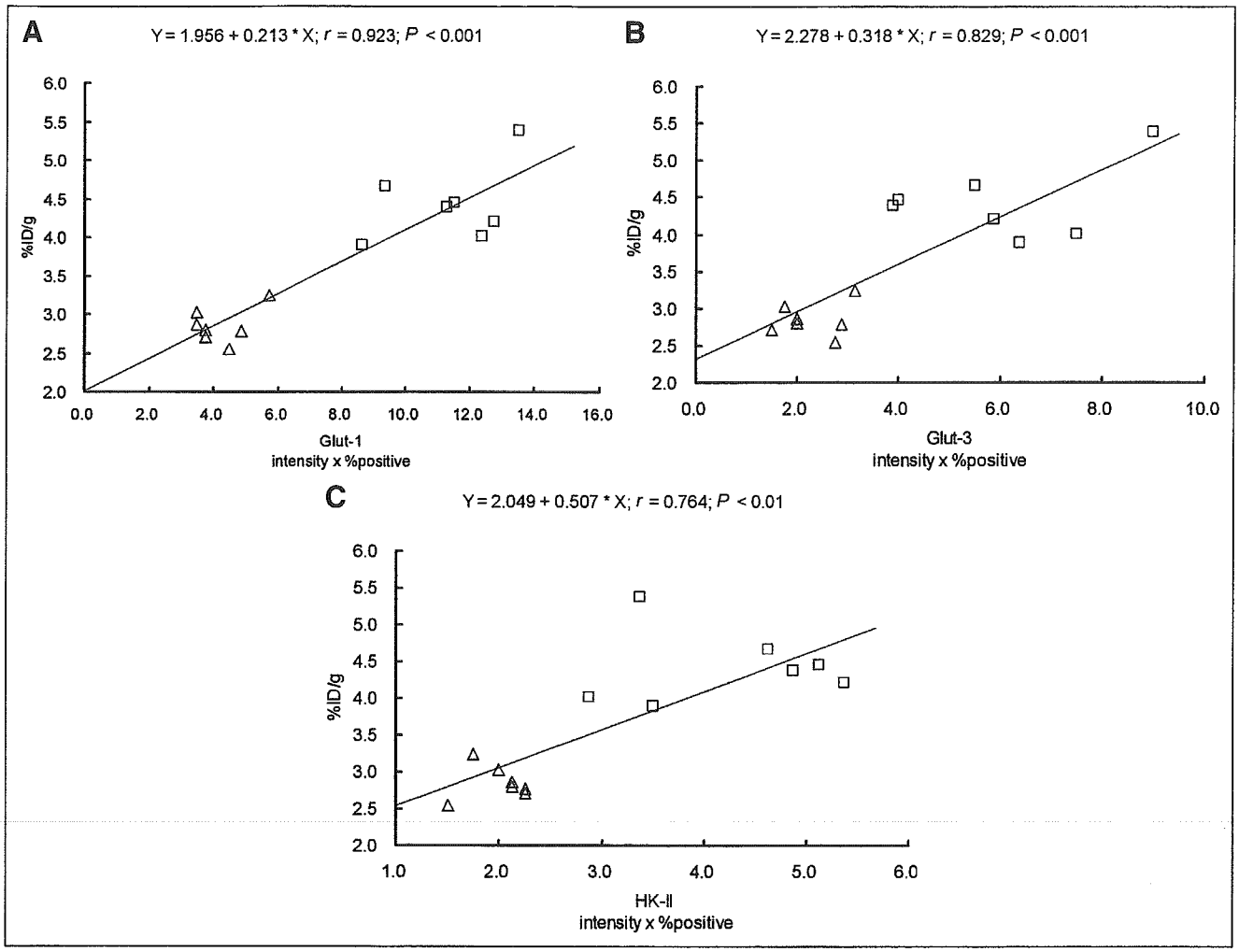

FIGURE 6. Relationships between expression levels of Glut-1, Glut-3, and HK-II and intratumoral ^{18}F-FDG accumulation in KDH-8 tumor tissues. Intratumoral ^{18}F-FDG accumulation significantly correlated with expression levels of Glut-1, Glut-3, and HK-II (intensity × % positive). (A) Relationship between ^{18}F-FDG accumulation and histochemical grading score for Glut-1. (B) Relationship between ^{18}F-FDG accumulation and histochemical grading score for Glut-3. (C) Relationship between ^{18}F-FDG accumulation and histochemical grading score for HK-II. □, CT region; △, PT region.

Although intratumoral heterogeneity in ^{18}F-FDG distribution has been demonstrated (*15*), there have been few reports with regard to the biologic mechanisms involved in the intratumoral heterogeneous distribution of ^{18}F-FDG. The present results showed a significant correlation between the intratumoral distribution of ^{18}F-FDG and the regional expression level of Glut-1, which is consistent with the results of syngeneic rat mammary cancer reported by Brown et al. (*30*). In addition, our results demonstrated—to our knowledge, for the first time—that intratumoral ^{18}F-FDG distribution significantly correlates with the regional expression levels of Glut-3 and HK-II. The heterogeneity in ^{18}F-FDG distribution may be ascribed to the altered expression levels of Glut-1, Glut-3, and HK-II and may reflect a metabolic microenvironment of tumors.

Aggressive tumors often have insufficient blood supply. Hypoxia occurs in tissue that is >100–200 μm away from a functional blood supply. When the tumors are exposed to a hypoxic environment, HIF-1α is activated to promote the transcription of several genes, including glucose transporters and glycolytic enzymes (*31*). The increased uptake of ^{3}H-FDG in vitro by hypoxic tumor cells has been well demonstrated (*32*). Recently, Dearling et al. (*33*) have extended the previous in vitro work and confirmed the selectivity of ^{18}F-FDG for hypoxic regions over normoxic regions in vivo. In the present study, a relatively higher ^{18}F-FDG accumulation was observed in the CT region, with elevated expression levels of Glut-1, Glut-3, and HK-II. The positive staining of HIF-1α was observed in these regions. Taken altogether, the regional expression levels of Glut-1, Glut-3, and HK-II may be increased by HIF-1α in a hypoxic environment within the tumor tissue and may contribute to the elevated ^{18}F-FDG accumulation.

Several studies have focused on the expression of Gluts and hexokinase activity to define the role of these proteins in the regulation of ^{18}F-FDG accumulation (*34,35*). Elevated expression levels of Glut-1 and Glut-3 are considered to be factors that contribute to the accumulation of ^{18}F-FDG in malignant tumors (*9–13,23,28*). It has also been suggested that the activity level of HK-II contributes to ^{18}F-FDG accumulation in various malignant tumors (*14*). Chromatographic, polyclonal antibody, and amino acid analyses indicated that rat hepatoma hexokinase is most closely related to HK-II and suggests that mitochondrial hexokinase activity determines the rate of accumulation of ^{18}F-FDG in tumors (*36*). These studies, however, used PET or tissue-counting techniques and correlated average ^{18}F-FDG accumulation in the tumor with protein expression. The biologic mechanisms involved in intratumoral heterogeneity in ^{18}F-FDG distribution have not been fully investigated. The present results demonstrate that the expression levels of Glut-1, Glut-3, and HK-II also contribute to intratumoral heterogeneity in ^{18}F-FDG distribution in our model rats, as determined using an ARG technique. It is crucial to consider the relative contributions of Glut-1, Glut-3, and HK-II to intratumoral ^{18}F-FDG accumulation. Unfortunately, we could not determine the relative contributions of these proteins, mainly due to the limited number of samples used in this study. Further studies are required to clarify the respective contributions of glucose transporters and hexokinase to intratumoral heterogeneity in ^{18}F-FDG accumulation.

Intratumoral ^{18}F-FDG distribution has been described at the cellular level by several investigators (*15–20*). Kubota et al. showed that ^{18}F-FDG preferentially accumulates in macrophages and young granulation tissues surrounding necrotic foci rather than in tumor cells using a malignant tumor mouse model (*15*). In contrast, Brown et al. (*17*) observed relatively less ^{3}H-FDG accumulation in necrotic/inflammatory infiltration compared with that in the tumor cells. Our results in rats confirmed intratumoral heterogeneity in ^{18}F-FDG distribution. The ^{18}F-FDG accumulation in the CT regions was 1.6 and 2.3 times higher than those in the PT and NA regions, respectively. Our results are consistent with the results reported by Brown et al.

In this study, the regions of viable tumor tissues and NA regions in ARG were identified using the HE-stained sections as reference. Apoptosis was most reliably assayed by morphologic counts using HE staining. Since there are some apoptotic cancer cells interwoven in necrotic regions and it was difficult to clearly distinguish apoptotic cells from necrotic cells in the present study, the term NA regions is used. Viable tumor cells and necrotic/apoptotic cells were also interwoven; thus, we used relatively small ROIs to clearly divide the regions between the viable tumor cells and necrotic/apoptotic cells. The larger ROIs appeared to cover both of the viable tumor cells and necrotic/apoptotic cells. Brown et al. (*17*) also used such ROI analysis to evaluate intratumoral distribution of ^{18}F-FDG. On the other hand, because necrotic cells revealed cell injuries in morphology—such as the cell membrane appearing ruptured, the nuclear chromatin being markedly condensed or pyknotic, vesicular structures filling the cytoplasm, and fusion of organelles (*37*)—the immunohistochemical staining of Glut-1, Glut-3, and HK-II cannot reflect the antigenicity of cells. Therefore, the expression levels of Glut-1, Glut-3, and HK-II were not investigated by immunostaining and semiquantitative evaluation in the NA regions. The slices immunohistochemically stained for Glut-1, Glut-3, and HK-II were from the formalin-fixed, paraffin-embedded specimens, but those used in ARG imaging to determine regional ^{18}F-FDG distribution were from the frozen samples. Thus, selected areas in the immunohistochemical staining for Glut-1, Glut-3, and HK-II of the CT, PT, and NA regions were not exactly congruent with those for determining regional ^{18}F-FDG distribution on ARG imaging, although both formalin-fixed, paraffin-embedded specimens and frozen samples were adjacent. It is important to note that expression of Glut-1, Glut-3, and hexokinase II (as determined in this study) does not generally imply increased functional activity. Several studies have demonstrated that hexokinase bound to the mitochondrial membrane has a much higher catalytic activity than cytosolic hexokinase. Aloj et al. (*14*) have also indicated that ^{18}F-FDG uptake correlates better with ^{18}F-FDG phosphorylating activity of mitochondrial preparations than with the level of expression of the Glut-1 or hexokinase I or II genes. The excellent correlation between HK-II expression and ^{18}F-FDG uptake observed in the present study may not be representative for other tumor models.

In our study, ARG imaging was performed 1 h after ^{18}F-FDG injection. The 1-h time point is widely used also in rodent models, and no significant differences in the ^{18}F-FDG uptake were observed in the mouse tumor tissues between 1 and 2 h after ^{18}F-FDG injection (*33*). However, further studies at more than one time point are needed to give an indication of the time course of ^{18}F-FDG uptake and to compare with the present results in rodent-bearing xenografts.

^{18}F-FDG PET has become increasingly important not only for detecting and staging malignant tumors but also for monitoring therapy response and for differentiating malignant lesions from benign lesions (*1–4*). However, variable tumor accumulation of ^{18}F-FDG has been indicated to prevent accurate diagnosis by ^{18}F-FDG PET (*38,39*). Intratumoral heterogeneity in ^{18}F-FDG distribution may also affect such diagnostic accuracy. The present study provides a biologic basis of intratumoral heterogeneity in ^{18}F-FDG distribution, which leads to better understanding of the mechanism of ^{18}F-FDG accumulation in tumors and contributes to the accurate diagnosis of patients with malignant tumors by ^{18}F-FDG PET. On the other hand, recent advances in radiation therapy such as intensity-modulated radiation therapy have exploited new areas for the use of

^{18}F-FDG PET (*40*). Regions of high ^{18}F-FDG uptake can be treated with a higher radiation dose compared with a hypometabolic portion of the same mass. In addition, glucose transporters (Glut-1 and Glut-3) and glycolytic enzymes (for example, hexokinase) are promoted by activated HIF-1α (*31*). The present study showed an excellent correlation between regional ^{18}F-FDG uptake and the expression of facilitative glucose transporters (Glut-1 and Glut-3) and HK-II. Furthermore, this study found that ^{18}F-FDG uptake was more intense in tumor regions that express HIF-1α. Recent clinical data indicate that hypoxic tumors are known to be more malignant, to be more likely to metastasize, and to have a poor prognosis. HIF-1α is considered to be a key factor for tumor progression by upregulating genes involved in angiogenesis, cell survival, cell invasion, and resistance to drug therapy and radiotherapy. Thus, the findings of this study suggest that tumor areas with high ^{18}F-FDG uptake may represent biologically more aggressive cancer cells. This has important consequences for the use of ^{18}F-FDG PET for treatment planning—particularly, intensity-modulated radiation therapy. ^{18}F-FDG PET could help to identify regions for dose-escalation protocols. We believe that our data also provide useful information in a precision radiation therapy protocol with modern radiotherapy modalities.

CONCLUSION

The colocalization of a high ^{18}F-FDG level and Glut-1, Glut-3, and HK-II overexpression in regions that are likely to be subjected to hypoxia as well as the strong correlation between the transporters and HK-II expression and ^{18}F-FDG accumulation suggest that enhanced transmembrane transport and phosphorylation may be part of an adaptive mechanism triggered by changes in the metabolic microenvironment of cancer cells. The regional expression levels of Glut-1, Glut-3, and HK-II may increase in a hypoxic environment within tumor tissues and may contribute to intratumoral heterogeneous ^{18}F-FDG distribution. The present results lead to a better understanding of the mechanism of ^{18}F-FDG accumulation in tumors, which may help in interpreting ^{18}F-FDG accumulation in patients with malignant tumors.

ACKNOWLEDGMENTS

This work was supported in part by a grant-in-aid for Scientific Research from the Japan Society for the Promotion of Science and in part by the Japanese Ministry of Education, Culture, Sports, Science and Technology and by a grant from the Rotary Yoneyama Memorial Foundation, Inc. The authors are grateful to the staff of the Nuclear Medicine and Central Institute of Isotope Science, Hokkaido University, for supporting this work. We also thank Mr. Kenichi Nishijima for technical assistance.

REFERENCES

1. Delbeke D, Rose DM, Chapman WC, et al. Optimal interpretation of FDG PET in the diagnosis, staging and management of pancreatic carcinoma. *J Nucl Med.* 1999;40:1784–1791.
2. Higashi T, Sakahara H, Torizuka T, et al. Evaluation of intraoperative radiation therapy for unresectable pancreatic cancer with FDG PET. *J Nucl Med.* 1999; 40:1424–1433.
3. Schelling M, Avril N, Nahrig J, et al. Positron emission tomography using [^{18}F]fluorodeoxyglucose for monitoring primary chemotherapy in breast cancer. *J Clin Oncol.* 2000;18:1689–1695.
4. Dimitrakopoulou-Strauss A, Strauss LG, Heichel T, et al. The role of quantitative ^{18}F-FDG PET studies for the differentiation of malignant and benign bone lesions. *J Nucl Med.* 2002;43:510–518.
5. Haberkorn U, Ziegler SI, Oberdorfer F, et al. FDG uptake, tumor proliferation and expression of glycolysis associated genes in animal tumor models. *Nucl Med Biol.* 1994;21:827–834.
6. Golshani-Hebroni SG, Bessman SP. Hexokinase binding to mitochondria: a basis for proliferative energy metabolism. *J Bioenerg Biomembr.* 1997;29:331–338.
7. Bell GI, Burant CF, Takeda J, Gould GW. Structure and function of mammalian facilitative sugar transporters. *J Biol Chem.* 1993;268:19161–19164.
8. Brown RS, Leung JY, Kison PV, Zasadny KR, Flint A, Wahl RL. Glucose transporters and FDG uptake in untreated primary human non-small cell lung cancer. *J Nucl Med.* 1999;40:556–565.
9. Reske SN, Grillenberger KG, Glatting G, et al. Overexpression of glucose transporter 1 and increased FDG uptake in pancreatic carcinoma. *J Nucl Med.* 1997;38:1344–1348.
10. Brown RS, Wahl RL. Overexpression of Glut-1 glucose transporter in human breast cancer: an immunohistochemical study. *Cancer.* 1993;72:2979–2985.
11. Boado RJ, Black KL, Pardridge WM. Gene expression of Glut-3 and Glut-1 glucose transporters in human brain tumors. *Brain Res Mol Brain Res.* 1994;27: 51–57.
12. Younes M, Brown RW, Stephenson M, Gondo M, Cagle PT. Overexpression of Glut-1 and Glut-3 in stage I nonsmall cell lung carcinoma is associated with poor survival. *Cancer.* 1997;80:1046–1051.
13. Suzuki T, Iwazaki A, Katagiri H, et al. Enhanced expression of glucose transporter Glut-3 in tumorigenic HeLa cell hybrids associated with tumor suppressor dysfunction. *Eur J Biochem.* 1999;262:534–540.
14. Aloj L, Caracó C, Jagoda E, Eckelman WC, Neumann RD. Glut-1 and hexokinase expression: relationship with 2-fluoro-2-deoxy-D-glucose uptake in A431 and T47D cells in culture. *Cancer Res.* 1999;59:4709–4714.
15. Kubota R, Yamada S, Kubota K, Ishiwata K, Tamahashi N, Ido T. Intratumoral distribution of fluorine-18-fluorodeoxyglucose in vivo: high accumulation in macrophages and granulation tissues studied by microautoradiography. *J Nucl Med.* 1992;33:1972–1980.
16. Kubota R, Kubota K, Yamada S, Tada M, Ido T, Tamahashi N. Microautoradiographic study for the differentiation of intratumoral macrophages, granulation tissues and cancer cells by the dynamics of fluorine-18-fluorodeoxyglucose uptake. *J Nucl Med.* 1994;35:104–112.
17. Brown RS, Leung JY, Fisher SJ, Frey KA, Ethier SP, Wahl RL. Intratumoral distribution of tritiated fluorodeoxyglucose in breast carcinoma. I. Are inflammatory cells important? *J Nucl Med.* 1995;36:1854–1861.
18. Kubota R, Kubota K, Yamada S, Tada M, Ido T, Tamahashi N. Active and passive mechanisms of [fluorine-18]fluorodeoxyglucose uptake by proliferating and prenecrotic cancer cells in vivo: a microautoradiographic study. *J Nucl Med.* 1994;35:1067–1075.
19. Kubota R, Kubota K, Yamada S, et al. Methionine uptake by tumor tissue: a microautoradiographic comparison with FDG. *J Nucl Med.* 1995;36:484–492.
20. Reinhardt MJ, Kubota K, Yamada S, Iwata R, Yaegashi H. Assessment of cancer recurrence in residual tumors after fractionated radiotherapy: a comparison of fluorodeoxyglucose, L-methionine and thymidine. *J Nucl Med.* 1997;38:280–287.
21. Zhao S, Kuge Y, Tsukamoto E, et al. Effects of insulin and glucose loading on FDG uptake in experimental malignant tumours and inflammatory lesions. *Eur J Nucl Med.* 2001;28:730–735.
22. Toorongian SA, Mulholland GK, Jewett DM, Bachelor MA, Kilbourn MR. Routine production of 2-deoxy-2-[^{18}F]fluoro-D-glucose by direct nucleophilic exchange on a quaternary 4-aminopyridinium resin. *Nucl Med Biol.* 1990;17: 273–279.
23. Zhao S, Kuge Y, Tsukamoto E, et al. Fluorodeoxyglucose uptake and glucose transporter expression in experimental inflammatory lesions and malignant tumours: effects of insulin and glucose loading. *Nucl Med Commun.* 2002;23:545–550.

24. Toyama H, Ichise M, Liow JS, et al. Absolute quantification of regional cerebral glucose utilization in mice by ^{18}F-FDG small animal PET scanning and 2-^{14}C-DG autoradiography. *J Nucl Med.* 2004;45:1398–1405.
25. Higashi T, Saga T, Nakamoto Y, et al. Relationship between retention index in dual-phase ^{18}F-FDG PET, and hexokinase-II and glucose transporter-1 expression in pancreatic cancer. *J Nucl Med.* 2002;43:173–180.
26. Zhong H, De Marzo AM, Laughner E, et al. Overexpression of hypoxia-inducible factor 1α in common human cancers and their metastases. *Cancer Res.* 1999;59: 5830–5835.
27. Higashi T, Tamaki N, Honda T, et al. Expression of glucose transporters in human pancreatic tumors compared with increased FDG accumulation in PET study. *J Nucl Med.* 1997;38:1337–1344.
28. Mochizuki T, Tsukamoto E, Kuge Y, et al. FDG uptake and glucose transporter subtype expressions in experimental tumor and inflammation models. *J Nucl Med.* 2001;42:1551–1555.
29. Bos R, Zhong H, Hanrahan CF, et al. Levels of hypoxia-inducible factor-1α during breast carcinogenesis. *J Natl Cancer Inst.* 2001;93:309–314.
30. Brown RS, Leung JY, Fisher SJ, Frey KA, Ethier SP, Wahl RL. Intratumoral distribution of tritiated-FDG in breast carcinoma: correlation between Glut-1 expression and FDG uptake. *J Nucl Med.* 1996;37:1042–1047.
31. Dang CV, Semenza GL. Oncogenic alterations of metabolism. *Trends Biochem Sci.* 1999;24:68–72.
32. Clavo AC, Brown RS, Wahl RL. Fluorodeoxyglucose uptake in human cancer cell lines is increased by hypoxia. *J Nucl Med.* 1995;36:1625–1632.
33. Dearling JL, Flynn AA, Sutcliffe-Goulden J, et al. Analysis of the regional uptake of radiolabeled deoxyglucose analogs in human tumor xenografts. *J Nucl Med.* 2004;45:101–107.
34. Flier JS, Mueckler MM, Usher P, Lodish HF. Elevated levels of glucose transport and transporter messenger RNA are induced by *ras* or *src* oncogenes. *Science.* 1987;235:1492–1495.
35. Birnbaum MJ, Haspel HC, Rosen OM. Transformation of rat fibroblasts by FSV rapidly increases glucose transporter gene transcription. *Science.* 1987;235:1495–1498.
36. Smith TA. Mammalian hexokinases and their abnormal expression in cancer. *Br J Biomed Sci.* 2000;57:170–178.
37. Bell HS, Whittle IR, Walker M, Leaver HA, Wharton SB. The development of necrosis and apoptosis in glioma: experimental findings using spheroid culture systems. *Neuropathol Appl Neurobiol.* 2001;27:291–304.
38. Bos R, van Der Hoeven JJ, van Der Wall E, et al. Biologic correlates of ^{18}fluorodeoxyglucose uptake in human breast cancer measured by positron emission tomography. *J Clin Oncol.* 2002;20:379–387.
39. Oshida M, Uno K, Suzuki M, et al. Predicting the prognoses of breast carcinoma patients with positron emission tomography using 2-deoxy-2-fluoro[^{18}F]-D-glucose. *Cancer.* 1998;82:2227–2234.
40. Lucignani G, Jereczek-Fossa BA, Orecchia R. The role of molecular imaging in precision radiation therapy for target definition, treatment planning optimisation and quality control. *Eur J Nucl Med Mol Imaging.* 2004;31:1059–1063.

J. Radiat. Res., 46, 93–102 (2005)

Regular Paper

Real-time Imaging of Hypoxia-inducible Factor-1 Activity in Tumor Xenografts

Junye LIU[1,2], Runjiang QU[1,2], Masakazu OGURA[1], Toru SHIBATA[1], Hiroshi HARADA[1,3]* and Masahiro HIRAOKA[1]

Hypoxia/Hypoxia-inducible factor-1 (HIF-1)/Hypoxia-response element (HRE)/Pimonidazole/Destabilized Enhanced GFP (d2EGFP).

Hypoxia-inducible factor-1 (HIF-1) is responsible for various gene expressions related to tumor malignancy, such as metastasis, invasion and angiogenesis. Therefore, monitoring HIF-1 activity in solid tumors is becoming increasingly important in clinical and basic studies. To establish a convenient system for visualizing HIF-1 activity in tumor xenografts, we employed a promoter consisting of five copies of hypoxia response elements (5HRE), whose activity depends on HIF-1, and used a derivative of green fluorescence protein (d2EGFP) as a reporter gene. A human melanoma cell line, Be11, which contains the 5HRE-d2EGFP gene, showed fluorescence in response to hypoxia. The fluorescent intensity correlated inversely with the surrounding oxygen tension, and was time-dependent for the hypoxic treatment. Reoxygenation resulted in a rapid decrease in fluorescence due to the signal sequence for protein degradation encoded in d2EGFP, which enabled monitoring of HIF-1 activity in real-time. Heterogeneous fluorescence was observed in the solid tumor of a non-sacrificed tumor-bearing mouse. Immunohistochemical analysis confirmed that d2EGFP-expressing regions overlapped with the ones stained with a hypoxia marker, pimonidazole. These results suggest that the 5HRE-d2EGFP gene is suitable for the real-time imaging of HIF-1-activating cells *in vivo*, due to the short half-life of the d2EGFP protein as well as the specificity of the 5HRE promoter for HIF-1 activity.

INTRODUCTION

The rapid proliferation and high metabolic demands of cancer cells cause a reduction in oxygen tension to below physiological levels, which is a typical feature of solid tumors and is known as tumor hypoxia.[1,2] In hypoxic tumor cells, a transcriptional factor, hypoxia-inducible factor-1 (HIF-1), induces various kinds of gene expression related to angiogenesis[3] and glycolysis[4], and appears to play a critical role in the development of invasive and metastatic properties.[5] Moreover, HIF-1 activity is associated with the resistance of tumor cells against radiotherapy as well as chemotherapy.[6,7] For example, it has been demonstrated that ionizing radiation (IR) treatment up-regulates HIF-1 activity and induces vascular endothelial growth factor (VEGF) gene expression in tumor cells, which then leads to radioresistance of endothelial cells and eventually to radioresistance of the tumor cells themselves.[8] In addition, significant associations between HIF-1 activity and patient mortality have been reported in clinical studies of brain[9], breast[10,11], cervix[12], oropharynx[13], ovarian cancer[14] *etc.*

HIF-1 is a heterodimeric transcriptional factor composed of α subunit (HIF-1α) and β subunit (HIF-1β), which is also known as ARNT (aryl hydrocarbon receptor nuclear translocator).[15] HIF-1α expression is regulated in an oxygen-dependent manner at the post-translational level and is responsible for the regulation of HIF-1 activity.[16] Under aerobic conditions, the proline residues, Pro-402 and Pro-564, in the oxygen dependent degradation (ODD) domain of HIF-1α protein are hydroxylated by prolyl hydroxylase-domain protein 1-3 (PHD1-3).[17,18] The modified HIF-1α protein is recognized as a target for ubiquitylation by E3 ubiquitin-protein ligases containing the von Hippel-Lindau tumor suppressor protein (pVHL).[17,18] Consequently, the ubiquitylated HIF-1α is degraded by the 26S proteasome.[17,18] On the other hand, the rate of prolyl hydroxylation decreases under

*Corresponding author: Phone: +81-75-751-3417,
Fax: +81-75-751-9749,
E-mail: hharada@kuhp.kyoto-u.ac.jp
[1]Department of Therapeutic Radiology and Oncology, Kyoto University Graduate School of Medicine, Kyoto, Japan; [2]Department of Radiation Medicine, Fourth Military Medical University, Xi'an, China; [3]Horizontal Medical Research Organization, Kyoto University Graduate School of Medicine, Kyoto, Japan.
Junye LIU and Runjiang QU contributed equally to this work.